Principles and Modeling of Radiofrequency Coil Signal Detection and Image Production

William A. Edelstein
MRScience LLC, Schenectady, NY; and Case Western Reserve University, Cleveland, OH

The sensitivity of radiofrequency (rf) coils ultimately determines the spatial and contrast resolution of MRI. We want s to calculate the signal and noise as a function of position within the imaging sample for a given coil arrangement. Their quotient is the signal-to-noise ratio SNR.

We will discuss modeling of a simple, single-loop rf receive coil and then explore the connection between the elements of the coil and physical reality. We will then briefly describe how these procedures are extended to more complicated receive coil arrangements.

Resonant rf coil electrical circuit [1-3]

Figure 1 shows the equivalent circuit of a single resonant rf coil. This applies to a simple loop surface coil or a single mode of a volume coil.

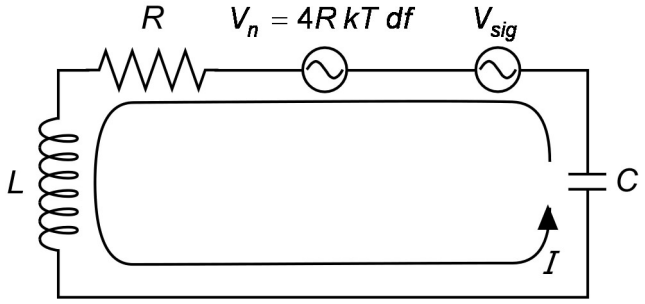

Figure 1. Resonant rf coil circuit. The inductance L resonates with the capacitance C. The NMR signal from the target volume is V_{sig}. This must compete with the noise voltage $V_n^2 = 4RkT\,df$ from the equivalent resistance R.

The coil inductance (or equivalent inductance) L resonates with net capacitance C. There also must be electrical losses in the coil and the sample represented by the resistance R. There is a voltage V_{sig} –the NMR signal—picked up from some sample voxel. V_{sig} must compete with the Johnson noise

$$V_n^2 = 4RkT\,df\,, \tag{1}$$

where Boltzmann's constant $k = 1.38 \text{ X } 10^{-23}\text{J/K}$, T is the temperature of the imaging subject and/or rf coil in Kelvin and df is the observational bandwidth in hertz.

An important concept for such a circuit is the Q. Q has many meanings and definitions: $Q = 2\pi \times \text{Energy stored}/\text{Energy loss per cycle}$; $Q = f/\Delta f$, where Δf is the frequency bandwidth of the resonant circuit. In terms of the circuit elements

$$Q = \frac{\omega L}{R} \tag{2}$$

Suppose we have a 10 cm diameter surface coil made from 5 mm diameter wire ($L \approx 193\,\text{nH}$) and that against the sample it has $Q \approx 30$. Then $R \approx 2.6\,\Omega$. Assuming $T \sim 300\,\text{K}$ and $df \sim 500\,\text{Hz}$, we use Eqn. 1 to obtain

$$V_n \sim 4.6\,\text{nV} \tag{3}$$

The *power* signal-to-noise ratio for Figure 1 is given by

$$SNR_p = \frac{V_{sig}^2}{V_n^2} \tag{4}$$

We now refine this model as shown in Figure 2.

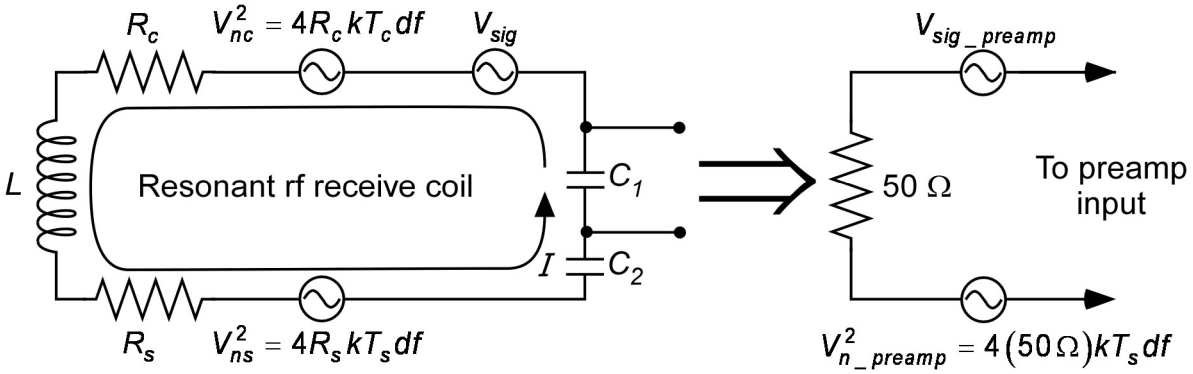

Figure 2. Full receive coil circuit model. The resonant receive coil includes losses (R_C) and thermal electrical noise from the coil and from the imaging sample (R_S). The output capacitor has been split into two parts to transform the output impedance to 50 Ω, the preferred source impedance for the preamplifier. The circuit to the right of the large arrow shows the equivalent circuit as seen by the preamplifier.

We can now be more specific about the sources of circuit resistance. First, the coil itself, typically made of copper, has resistive losses which produce electrical noise. This is represented by resistance R_c. When a sample/person is inserted into a body or head coil, or a surface coil is placed against the body, the coil acquires an additional resistance R_s which increases the total thermal noise.

We can understand R_s as follows. A current at the receive frequency through the receive coil would produce oscillating fields in the body. These fields would cause currents to flow and, since the body is a lossy conductor, the resultant losses would look like a resistance to the originating coil.

From another viewpoint, the body must have fluctuating, thermally-driven currents, and these produce fields which are in turn picked up by the receive coil. These must be the same as calculated from the Johnson noise formula for the resistance R_s according to the "fluctuation-dissipation" theorem.

Electrical noise from the body is inescapable. The best one can do is to have only noise from the body and none from dissipation in the coil. It is therefore desirable to make R_c small compared to R_s. Recall that the series $R \sim 1/Q$. Rf designers often say that they want the Q

to drop by a factor of 5 or more when the imaging sample is placed within or next to the receive coil. The comparison between the ideal amount of noise and noise included from the coil is given by

$$\text{noise power ratio} = \frac{R_s + R_c}{R_c} = \frac{Q_{empty}/Q_{loaded}}{Q_{empty}/Q_{loaded} - 1} \tag{5}$$

For $Q_{empty}/Q_{loaded} = 5$, the noise power ratio[1] is 1.25 or 0.97 dB. Thus the intrinsic resistance of the copper in the coil contributes an extra 25% noise power and decreases the power SNR by 25%. This can be compared to the 0.5 dB noise figure of a reasonable preamplifier which must contribute an extra 12% noise power.[2]

It is possible to decrease the coil resistance dramatically by using cold copper (for example, at liquid nitrogen temperature, 77K [4-7]) or almost to zero by the use of superconducting material in the coil [8-14]. These techniques may be useful when it otherwise difficult to get a large Q ratio, for example, in MRI of small animals or MRI microscopy.

To maximize performance, the output capacitor is divided in order to transform the output impedance to 50 Ω, the optimum source impedance for the preamplifier. The signal and noise are transformed by the same amount, so the SNR (signal-to-noise ratio) is the same in the equivalent preamplifier input circuit on the right as it was in the receive circuit.

NMR sensitivity

To illustrate the basic ideas of sensitivity modeling, we calculate the NMR sensitivity for a circular loop surface coil placed on a half-space of muscle tissue. The plane of the coil is parallel to the static field $\mathbf{B}_0$.

Power dissipation

In order to determine the sample noise resistance R_s, we need to calculate the losses in the material given unit current I in the circuits in Figs. 1 and 2.

The power dissipation per unit volume for currents induced in the sample, averaged over a cycle of current is

$$\frac{dP}{dV} = \frac{1}{2}\mathbf{j}\cdot\mathbf{E} \tag{6}$$

where $\mathbf{j}$ is the current density and $\mathbf{E}$ is the induced electric field. Since $\mathbf{j} = \sigma\mathbf{E}$ and $\mathbf{E} = -\omega\mathbf{A}$, we can get the resistance by evaluating

$$R_s = \frac{P}{(1\,\text{A})^2} = \frac{\sigma\omega^2}{2}\int \left|\frac{\mathbf{A}}{I}\right|^2 dV \tag{7}$$

---

[1] Decibels or dB are calculated from a quantity X as $10\log(x)$.

[2] The *noise amplitude ratio* is given by $\sqrt{1.25} = 1.12$. Thus the non-zero resistance in the copper coil increases the noise amplitude (and decreases the SNR) by 12%.

A circular loop only has an azimuthal component, ([15], p. 270-271):

$$\frac{A_\phi}{I} = \frac{\mu 0}{\pi k}\left(\frac{a}{r}\right)^{1/2}\left[\left(1-½k^2\right)K - E\right],\ k^2 = \frac{4ar}{\left[(a+r)^2+z^2\right]} \tag{8}$$

where K and E are complete elliptic integrals of the first and second kind. a is the coil radius, r is the cylindrical (transverse) radius, and z is the perpendicular distance from the coil plane.

Because the vector potential is azimuthally symmetric, the integral over ϕ can be done immediately and in Eq. 7 becomes

$$R_s = \pi\sigma\omega^2\int_{z0}^{\lim 1}\int_0^{\lim 2}\left(\frac{A_\phi}{I}\right)^2 r\,dr\,dz \tag{9}$$

where lim1 and lim2 are chosen to be large enough so the integral converges.

Eq. 9 can be numerically integrated (I did it in Mathcad). Suppose our 10 cm diameter circular loop coil is 5 mm off the surface of a conducting half-volume, so $z0 = 5\ \text{mm}$. Take the volume conductivity to be approximately 0.7 S/m (the value for muscle at 50 MHz [16]).

The answer is

$$R_s = 3.0\ \Omega \tag{10}$$

which gives for the noise voltage from Eq. 1

$$V_n \sim 5.0\ \text{nV} \tag{11}$$

Signal Voltage

The coil signal voltage for a small volume dV containing magnetization per unit volume M_0 is given by

$$\frac{V_{sig}}{dV} = \omega\, b_{1r}\, M_0, \tag{12}$$

where b_{1r} is the rotating field component, perpendicular to the static field, created at the site of the small volume dV by unit current through the coil. This is the *reciprocity principal* [17-23].

Magnetization

We first calculate the magnetic moment per unit volume M_0 in Eq. 12. This is given by [18]

$$M_0 = \frac{N\gamma_n^2\hbar^2 I(I+1)}{3kT}\bullet B_0 \tag{13}$$

where water proton density $N = 6.69\times 10^{29}\ \text{protons/m}^3$, $\gamma_n = 2.68\times 10^8\ \text{Hz/T}$, $\hbar = 1.055\times 10^{-34}\ \text{J}\cdot\text{s}$, spin $I = 1/2$. At $T = 300\ \text{K}$ and static field $B_0 = 1.5\ \text{T}$, we get

$$M_0 = 3.1\times 10^{-3}\,\frac{\text{A}\cdot\text{m}^2}{\text{m}^3} \tag{14}$$

Calculating b_1

In principal, the magnetic field $\mathbf{B}$ can be calculated at any point by integrating the *Biot-Savart law* [1]*:*

$$d\mathbf{B} = \frac{\mu 0\, I}{4\pi r^3}\mathbf{r} \otimes d\mathbf{s} \tag{15}$$

where $\mu 0 = 4\pi \times 10^{-7}\ \mathrm{H/m}$ is the magnetic permeability of free space, $\mathbf{r}$ is the vector from a current element to the target point, I is the current and $d\mathbf{s}$ is the infinitesimal vector along the current element.

In the case of the circular loop, Eq. 15 can be integrated analytically ([15], pp. 270-271). The general result is given in terms of elliptic integrals.

We will calculate the signal and SNR along the axis of the circular loop. In this case the rotating magnetic field along the axis simplifies to [15]

$$b_{1r} = \frac{1}{4}\frac{\mu 0 a^2}{\left(a^2 + z^2\right)^{3/2}} \tag{16}$$

where a is the coil radius and z is the distance from the loop plane to the evaluation point. We have divided the formula in Smythe [15] by 2 in order to get the rotating component.

Using Eq. 16, we calculate the field at a depth of 10 cm for a 10 cm diameter coil and get

$$b_{1r}\left(10\ \mathrm{cm}\right) = 0.562\ \mu\mathrm{T/A} \tag{17}$$

Putting this value for the rotating field into Eq. 12, we get

$$V_{sig}\left(10\ \mathrm{cm}\right) = 700\ \mathrm{nV/cm^3} \tag{18}$$

Making an image

The information derived above can be used in many ways, and there are many factors to take into account when modeling image production.

Suppose that a particular pulse sequence has 128 data acquisition repetitions. Leaving aside relaxation time effects (one of those factors), the equivalent noise voltage from Eq. 11 is decreased to

$$V_n^{128} \sim \frac{5.0\ \mathrm{nV}}{\sqrt{128}} = 0.44\ \mathrm{nV} \tag{19}$$

We can immediately see that, for 1 $\mathrm{mm^3}$, the signal from Eq. 18 decreases by a factor of 1000, and the $\mathrm{SNR} \sim 0.7/0.44 = 1.6$ (Eq. 18/Eq. 19), just below a detection limit of $\mathrm{SNR} \sim 2$.

We can calculate the SNR as a function of depth in the sample for this set of parameters. The result is shown in Fig. 3.

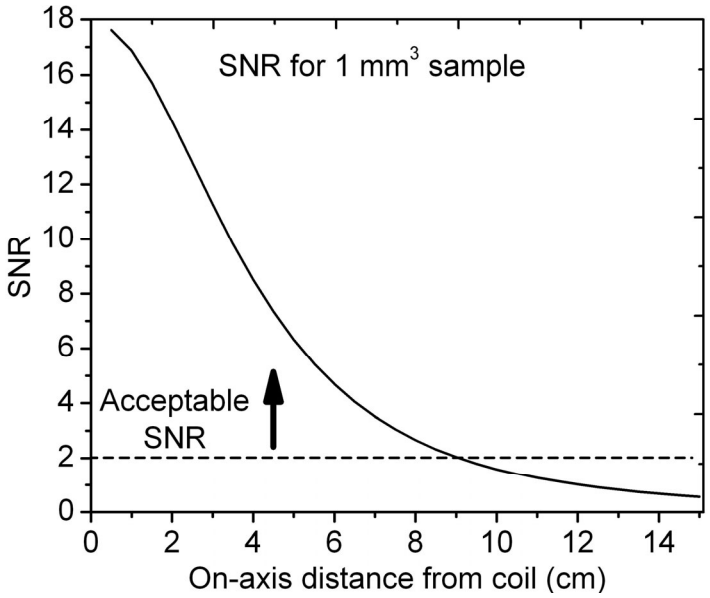

Figure 3. SNR for 1 mm^3 sample as a function of distance from a 10 cm diameter surface coil. The sample boundary starts at 5 mm from the plane of the surface coil. Some parameters of interest: bandwidth 500 Hz; 128 data acquisitions; sample $\sigma = 0.7$ S/m.

It is apparent that reasonable SNR will be obtained for voxels less than 9 cm from the coil.

This information can all be rescaled for different voxel volumes and pulse sequences. Relaxation times must be taken into account. The field of view of such pictures can be extended using knowledge of the rf field. Ideally, effects of variations of the static and gradient fields should also be included. Thus image simulation is very complex.

Phased arrays and volume coils

Phased arrays are combinations of individual surface coils, and their sensitivity maps can be combined according to the rules for making images. The input to a volume coil can be modeled as an equivalent circuit such as Fig. 2.

Eddy current effects

The notional applied field from the receive coil will induce eddy currents which, in turn, will produce fields that affect the sensitivity map. This effect becomes increasingly important as the static field strength and corresponding NMR frequency increases [19, 22, 23]. In the presence of eddy currents, it is also necessary to calculate the sensitivity using the counter-rotating field [19, 22, 23].

Numerical calculations

It is evident that calculations such as those contained in this note are complex, even for the very simple geometry we have chosen. More varied geometries, such as phased arrays, volume coils, or a sample such as the human body with its irregular regions, requires a numerical computational approach such as FDTD or electromagnetic finite element software (e.g. [24-32]).

Acknowledgements

I would like to thank Dr. Chris Collins of Penn State, Dr. Chris Hardy of GE and Dr. John Schenck of GE for helpful discussions.

References

1. BI Bleaney and B Bleaney, *Electricity and Magnetism*. 3rd ed. Vol. 1. 1993, Oxford, UK: Oxford University Press.
2. CD Motchenbacher and JA Connelly, *Low-Noise Electronic System Design*. 1993, New York, USA: John Wiley & Sons.
3. BL Sorgenfrei and WA Edelstein, "Optimizing MRI signal-to-noise ratio for quadrature unmatched RF coils: Two preamplifiers are better than one." *Magnetic Resonance in Medicine* **36,** p. 104-110 (1996).
4. JC Smith and RL Nunnally, "Improvement in SNR at 3T Using a LN2 Cooled Copper RF Coil" in *Proc. Intl. Soc. Mag. Reson. Med. 11*. 2004: Intl. Soc. Mag. Reson. Med., p. 42.
5. JC Smith, RL Nunnally, K McGuigan, and JH Postlethwait, "Magnetic Resonance Imaging of Stickleback Fish Brains Using Cryo-Cooled Surface Coils" in *Proc. Intl. Soc. Mag. Reson. Med. 11*. 2004. Kyoto, Japan: Intl. Soc. Mag. Reson. Med., p. 2422.
6. L Xue, M Kamel, L Xie, J Wosik, and P Narayana, "SNR Limit for Cryogenic Arrays" in *Proc. Intl. Soc. Mag. Reson. Med. 13 (2005)*. 2005. Miami, FL, USA: Intl. Soc. Mag. Reson. Med., p. 2436.
7. EB Boskamp, SA Lindsay and JE Lorbiecki, "On the coil noise contribution to SNR versus coil diameter, temperature, frequency and load distance" in *Proc. Intl. Soc. Mag. Reson. Med. 13*. 2005. Miami, FL, USA: Intl. Soc. Mag. Reson. Med., p. 916.
8. RD Black, TA Early, PB Roemer, OM Mueller, A Mogrocampero, LG Turner, and GA Johnson, "A High-Temperature Superconducting Receiver For Nuclear-Magnetic-Resonance Microscopy." *Science* **259,** p. 793-795 (1993).
9. RD Black, TA Early and GA Johnson, "Performance Of A High-Temperature Superconducting Resonator For High-Field Imaging." *Journal Of Magnetic Resonance Series A* **113,** p. 74-80 (1995).
10. SE Hurlston, WW Brey, SA Suddarth, and GA Johnson, "A high-temperature superconducting Helmholtz probe for microscopy at 9.4 T." *Magnetic Resonance In Medicine* **41,** p. 1032-1038 (1999).
11. JR Miller, SE Hurlston, QY Ma, DW Face, DJ Kountz, JR MacFall, LW Hedlund, and GA Johnson, "Performance of a high-temperature superconducting probe for in vivo microscopy at 2.0 T." *Magnetic Resonance In Medicine* **41,** p. 72-79 (1999).
12. L Darrasse and JC Ginefri, "Perspectives with cryogenic RF probes in biomedical MRI." *Biochimie* **85,** p. 915-937 (2003).
13. HL Lee, IT Lin, JH Chen, HE Horng, and HC Yang, "High-Tc superconducting receiving coils for nuclear magnetic resonance imaging." *IEEE Transactions On Applied Superconductivity* **15,** p. 1326-1329 (2005).
14. JC Ginefri, M Poirier-Quinot, P Robert, and L Darrasse, "Contrast-enhanced dynamic MRI protocol with improved spatial and time resolution for in vivo microimaging of the mouse with a 1.5-T body scanner and a superconducting surface coil." *Magnetic Resonance Imaging* **23,** p. 239-243 (2005).
15. WR Smythe, *Static and Dynamic Electricity*. 1950, New York: McGraw-Hill.

16. CH Durney, H Massoudi and MF Iskander, Brooks Air Force Base, "Radiofrequency Radiation Dosimetry Handbook," pp. http://www.brooks.af.mil/AFRL/HED/hedr/reports/handbook/, 12/2/05.

17. DI Hoult and RE Richards, "Critical factors in the design of sensitive high resolution nuclear magnetic resonance spectrometers." *Proceedings of the Royal Society of London* **A. 344,** p. 311-340 (1975).

18. DI Hoult and PC Lauterbur, "The Sensitivity of the Zeugmatographic Experiment Involving Human Samples." *Journal of Magnetic Resonance* **34,** p. 425-433 (1979).

19. GH Glover, CE Hayes, NJ Pelc, WA Edelstein, OM Mueller, HR Hart, CJ Hardy, M O'Donnell, and WD Barber, "Comparison of linear and circular polarization for magnetic resonance imaging." *Journal of Magnetic Resonance* **64,** p. 255-270 (1985).

20. C-N Chen and DI Hoult, *Biomedical Magnetic Resonance Technology*. 1989, Bristol, UK: A. Hilger.

21. EM Haacke, RM Brown, MR Thompson, and R Venkatesan, *Magnetic Resonance Imaging: Physical Principles and Sequence Design*. 1999, New York, USA: John Wiley & Sons.

22. DI Hoult, "The principle of reciprocity in signal strength calculations: a mathematical guide." *Concepts in Magn. Reon.* **12,** p. 173-187 (2000).

23. CM Collins, QX Yang, JH Wang, X-H Zhu, G Adriany, S Michaeli, JT Vaughan, X Zhang, H Liu, P Anderson, K Ugurbil, MB Smith, and W Chen, "Different Excitation and Reception Distributions with a Single-Loop Transmit-Receive Surface Coil Near a Head-Sized Spherical Phantom at 300 MHz." *Magnetic Resonance in Medicine* **47,** p. 1026-1028 (2002).

24. RW Singerman, TJ Denison, H Wen, and RS Balaban, "Simulation of B-1 field distribution and intrinsic signal-to-noise in cardiac MRI as a function of static magnetic field." *Journal Of Magnetic Resonance* **125,** p. 72-83 (1997).

25. TS Ibrahim, R Lee, BA Baertlein, AM Abduljalil, H Zhu, and PML Robitaille, "Effect of RF coil excitation on field inhomogeneity at ultra high fields: A field optimized TEM resonator." *Magnetic Resonance Imaging* **19,** p. 1339-1347 (2001).

26. TS Ibrahim, R Lee, AM Abduljalil, BA Baertlein, and PML Robitaille, "Dielectric resonances and B-1 field inhomogeneity in UHFMRI: computational analysis and experimental findings." *Magnetic Resonance Imaging* **19,** p. 219-226 (2001).

27. JH Wang, QX Yang, XL Zhang, CM Collins, MB Smith, XH Zhu, G Adriany, K Ugurbil, and W Chen, "Polarization of the RF field in a human head at high field: A study with a quadrature surface coil at 7.0 T." *Magnetic Resonance In Medicine* **48,** p. 362-369 (2002).

28. CM Collins and MB Smith, "Spatial resolution of numerical models of man and calculated specific absorption rate using the FDTD method: A study at 64 MHz in a magnetic resonance imaging coil." *Journal Of Magnetic Resonance Imaging* **18,** p. 383-388 (2003).

29. WZ Liu, CM Collins, PJ Delp, and MB Smith, "Effects of end-ring/shield configuration on homogeneity and signal-to-noise ratio in a birdcage-type coil loaded with a human head." *Magnetic Resonance In Medicine* **51,** p. 217-221 (2004).

30. W Liu, CM Collins and MB Smith, "Calculations of B-1 distribution, specific energy absorption rate, and intrinsic signal-to-noise ratio for a body-size birdcage coil loaded with different human subjects at 64 and 128 MHz." *Applied Magnetic Resonance* **29,** p. 5-18 (2005).

31. BK Li, F Liu and S Crozier, "Focused, eight-element transceive phased array coil for parallel magnetic resonance imaging of the chest-theoretical considerations." *Magnetic Resonance In Medicine* **53,** p. 1251-1257 (2005).

32. CM Collins, WZ Liu, W Schreiber, QX Yang, and MB Smith, "Central brightening due to constructive interference with, without, and despite dielectric resonance." *Journal Of Magnetic Resonance Imaging* **21,** p. 192-196 (2005).